Published in final edited form as:
Magn Reson Med. 2006 December ; 56(6): 1384–1388. doi:10.1002/mrm.21093.

A Targeted PARACEST Nanoparticle Contrast Agent for the Detection of Fibrin

Patrick M. Winter[1], **Kejia Cai**[1], **Junjie Chen**[1], **Christopher R. Adair**[2], **Garry E. Kiefer**[2], **Phillip S. Athey**[3], **Patrick J. Gaffney**[4], **Carolyn E. Buff**[5], **J. David Robertson**[5], **Shelton D. Caruthers**[1,6], **Samuel A. Wickline**[1], and **Gregory M. Lanza**[1]

[1] Washington University, St. Louis, MO

[2] Macrocyclics, Dallas, TX

[3] The Dow Chemical Co., Freeport, TX

[4] St. Thomas' Hospital, London, UK

[5] University of Missouri Research Reactor, Columbia, MO

[6] Philips Medical Systems, Cleveland, OH

Abstract

A lipid-encapsulated perfluorocarbon nanoparticle molecular imaging contrast agent utilizing a PARAmagnetic Chemical Exchange Saturation Transfer (PARACEST) chelate is presented. PARACEST agents are ideally suited for molecular imaging applications because the contrast can be switched on and off at will simply by adjusting pulse sequence parameters. This obviates the need for pre- and post-injection images in order to define contrast agent binding. Spectroscopy (4.7 T) of PARACEST nanoparticles revealed a bound water peak at 52 ppm, in agreement with results from the water-soluble chelate. Imaging of control nanoparticles showed no appreciable contrast, while PARACEST nanoparticles produced >10% signal enhancement. PARACEST nanoparticles were targeted to clots via anti-fibrin antibodies and produced a contrast-to-noise ratio of 10 at the clot surface.

Keywords

MRI; contrast agent; nanoparticle; fibrin; molecular imaging

Myocardial disease and stroke continue to be the nation's leading killer, responsible for nearly 1 million (42%) of all American deaths annually. Of these losses, approximately 160,000 are individuals between 35 to 64 years of age (1) for whom the current early diagnosis techniques offered little effectiveness. New early detection strategies are needed to prevent a patient's first symptomatic presentation from being the last. Although a variety of invasive approaches can be used to characterize atherosclerotic plaques and follow their changes serially (2), these techniques are primarily confined to research studies due to the increased risk, cost, and time required.

We have proposed that early recognition and quantification of microthrombi in ruptured plaques could provide an important biomarker to justify and guide aggressive therapeutic

Corresponding Author: Patrick M. Winter, Ph.D., Washington University School of Medicine, 4320 Forest Park Blvd., Cortex Suite 101, Campus Box 8215, St. Louis, MO 63108, Ph: 314-454-8635, FAX: 314-454-7490, patrick@cvu.wustl.edu.

strategies to impede disease progression (3). We have reported the use of a lipid encapsulated, perfluorocarbon nanoparticle system for MR molecular imaging of fibrin, an abundant component of thrombus. The agent affords specific detection of fibrin deposits using paramagnetic gadolinium chelates on the surface (4–5). The highly amplified paramagnetic signal provides a robust way to image targeted nanoparticles, but routine use requires collection of pre- and post-injection images to determine signal changes.

Chemical exchange saturation transfer (CEST) agents have exchangeable protons (-NH, -OH, etc.) resonating at a chemical shift that is distinguishable from the bulk water signal. RF pre-pulses applied at the appropriate frequency and power level can saturate the exchangeable protons, which transfer into the bulk water pool and lead to reduced equilibrium magnetization (6). This imparts CEST agents with a unique ability in the realm of MRI of switching the image contrast “on” and “off” by simply changing the pulse sequence parameters. This can minimize the time delays and motion-induced artifacts inherent in normal pre- and post-contrast imaging protocols. Although several agents contain exchangeable protons and can produce CEST contrast (7), the chemical shifts are often very close to the bulk water signal, making it difficult to distinguish contrast due to saturation transfer versus direct saturation of the bulk water. Paramagnetic ions can be utilized to shift the bound water frequency further away from the bulk water, allowing distinct saturation of the exchangeable protons (8). These agents, termed PARACEST agents, consist of paramagnetic chelates specifically designed to exhibit exchangeable proton or bound water peaks and are emerging candidates for molecular imaging applications.

To date, previously reported supramolecular PARACEST agents have been symmetrical chelates coupled to cationic polymers through ion-pair attractions (9–10) or entrapped within a liposomal vesicle (11). The objectives of this study were to: 1) synthesize and demonstrate an asymmetric PARACEST chelate bifunctional-modified for chemical coupling to a lipid-encapsulated nanoparticle, 2) stably incorporate very high payloads of the lipid-conjugated PARACEST chelate into the nanoparticle surfactant, 3) measure the effectiveness of this PARACEST agent in suspension at 4.7 T, and 4) demonstrate the first fibrin-targeted PARACEST agent in vitro.

METHODS

Chelate Synthesis and Nanoparticle Formulation

In brief, the PARACEST chelate was based upon the 1,4,7,10-tetraaza macrocycle employing N-substituted glycine ethyl ester ligating moieties and a functionalized aromatic group for lipid conjugation (The Dow Chemical Co.) (Fig. 1). Europium was added at equimolar concentrations to form the PARACEST construct, Eu^{3+}-methoxy-benzyl-DOTA. A lipophilic tail, phosphatidylethanolamine (Avanti Polar Lipids, Inc.), was coupled to the compound through a thiourea linkage. Proton NMR spectroscopy was performed on the water soluble chelate (i.e., non-lipid conjugated) at 4.7 T revealing a distinct bound water peak at 52 ppm (data not shown), consistent with a previously reported symmetric PARACEST chelate (12).

Perfluorocarbon nanoparticles were produced similar to previous reports (4–5). The nanoparticles were prepared by emulsifying 15% (v/v) perfluorooctylbromide (PFOB; Minnesota Manufacturing and Mining), 1% (w/v) surfactant comixture, 2.5% (w/v) glycerin and water for the balance in a microfluidizer (Microfluidics, Inc.) for 4 minutes at 20,000 psi. PARACEST nanoparticle surfactant was comprised of phosphatidylcholine (Avanti Polar Lipids, Inc.), biotinylated dipalmitoylphosphatidylethanolamine (Avanti Polar Lipids, Inc.), and Eu^{3+}-methoxy-benzyl-DOTA at a molar ratio of 59:1:40, respectively. Control

nanoparticles lacked the europium chelate, which was substituted with an equivalent increase in phosphatidylcholine.

Particle size, using quasi-elastic light scattering, and zeta potential, based upon an electrophoretic light scattering/laser Doppler velocimetry method, was measured in deionized water at 25°C with a Brookhaven ZetaPlus analyzer (Brookhaven Instrument Corp.). The europium content of the emulsion was determined by standard comparator instrumental neutron activation analysis at the University of Missouri Research Reactor (MURR). Specifically, Eu^{3+} was quantified by measuring the 842 keV gamma ray from the beta decay of ^{152m}Eu ($t_{1/2}$ = 9.31 h) produced through neutron capture by ^{151}Eu. The samples and comparator standards were irradiated in a thermal flux of ~ 5×10^{13} n/(s*cm^2) for 60 seconds, allowed to decay for several hours, and counted on a high-resolution gamma-ray spectrometer for 30 minutes. The minimum detection limit for this procedure is 2 ng of Eu^{3+}.

PARACEST Imaging and Spectroscopy

Imaging and spectroscopy studies were performed on a 4.7 T Varian Inova scanner at room temperature (23°C) using a 3 cm diameter custom-built circular surface coil. Bulk water spectra were collected from both PARACEST and control nanoparticle samples (50 μl) using a 2 second presaturation pulse at a power level of 28 dB. The saturation frequency was stepped between ±100 ppm (relative to the bulk water frequency at 0 ppm) in 1 ppm increments and the bulk water signal was integrated using a Matlab program (The MathWorks, Inc.). The difference between the integrated signals measured at equivalent positive and negative saturation frequencies was plotted, yielding saturation transfer profiles for the PARACEST and control nanoparticles.

The effectiveness of the PARACEST nanoparticles was compared to control particles using a two-chamber phantom constructed with an inner 1 cm diameter chamber that contained the undiluted nanoparticle emulsion. The outer 1.8 cm diameter chamber contained phosphate buffered saline (PBS). Gradient echo images of the two-chamber phantom were collected using a 2.5 second presaturation pulse at a power level of 38 dB with a frequency offset of ±52 ppm relative to the bulk water peak. Other imaging parameters were: TR = 2.52 s, TE = 4.4 ms, number of averages = 8, in-plane resolution = 156 μm by 156 μm, slice thickness = 4mm. Image intensity was normalized with respect to the signal from the PBS chamber, images were subtracted pixel-by-pixel and saturation transfer signal enhancement was calculated. The signal enhancement of PARACEST nanoparticles was also measured following presaturation pulses of 1, 2 or 3 seconds duration at power levels of 26, 29, 32, 35 or 38 dB using low resolution imaging (TR = 3.1 s, TE = 2.9 ms, number of averages= 2, in-plane resolution = 390 μm by 390 μm, slice thickness = 4 mm).

The concept of a fibrin-targeted PARACEST nanoparticle was studied using cylindrical plasma clots suspended in sterile saline inside plastic snap-cap tubes. The acellular clots were formed in a 5 mm diameter plastic mold prepared by combining fresh dog plasma, 100 mM calcium chloride (3:1 v/v), and 5 U thrombin around a 4-0 silk suture. Clots were serially incubated with 150 μg biotinylated anti-fibrin antibodies (1H10) (13–15) overnight at 4°C, followed by 50 μg avidin for 1 hr at 25°C, and then 250 μl of PARACEST (n=5) or control (n=4) nanoparticles for 1 hr at 25°C to complete the binding. Clots were rinsed three times with sterile saline after each incubation step to remove unbound reactants. Gradient echo images were collected of each clot using identical parameters as used for the two-chamber phantom. The clot surface was manually traced in Matlab and the contrast-to-noise ratio (CNR) was calculated relative to the standard deviation of the image intensity in air. The tracing was repeated in triplicate for each clot by a single observer and averaged.

Statistical Analysis

All studies followed a completely randomized design. Data were analyzed by student's t-Test or ANOVA. Means were separated when appropriate using the least significant difference (LSD) method and declared significant at an alpha level of 0.05 using a beta level of 0.80. Unless otherwise specified, averages are presented as a mean ± SEM.

RESULTS

Incorporation of the Eu^{3+}-methoxy-benzyl-DOTA chelate into the nanoparticle surface produced an emulsion with similar physical characteristics as the control nanoparticles. PARACEST and control nanoparticles had similar diameters, 294 nm and 337 nm, and polydispersity, 0.215 and 0.093, respectively. These nominal particle sizes are modestly larger than previously reported (4,5) due to the lower percentage of surfactant lipids and perfluorocarbon utilized in this formulation. The apparent stability and effectiveness of these particles were unaffected by the slight increase in size. The concentration of Eu^{3+} in the PARACEST nanoparticle emulsion was 2.1 mM, whereas the control nanoparticles contained no detectable Eu^{3+}. The zeta potential of the control nanoparticles was −51.4 mV in deionized water, while the PARACEST nanoparticles were 53.8 mV, indicating that the Eu^{3+} chelate carries a significant positive charge.

PARACEST nanoparticles displayed a marked saturation transfer effect at a presaturation frequency of 52 ppm (Fig. 2). This corresponds to saturation of the bound water peak at 52 ppm, which is transferred into the bulk water and decreases the signal acquired at 0 ppm. Control nanoparticles, however, did not show any appreciable saturation transfer at this frequency.

Images of the two-chamber phantom collected with the saturation pulse at −52 ppm showed very similar signal intensity for PARACEST nanoparticles, control nanoparticles and PBS (Fig. 3). Subtracting images collected with saturation at +52 ppm from the −52 ppm images revealed uniform PARACEST enhancement in the inner chamber, which was not observed with either control nanoparticles or PBS. PARACEST nanoparticles provided an image enhancement of 11.17 ± 0.01% in comparison with the control nanoparticles, which provided very little contrast change (0.53 ± 0.01%, * $p < 0.05$).

Increasing the duration and/or power of the presaturation pulse augmented the image enhancement obtained with PARACEST nanoparticles (Fig. 4). While the best results are obtained with a very long, high power presaturation pulse, it is evident that even a 1 second pulse with a power of 35 dB could produce adequate signal change to be reliably detected in an image. Since the PARACEST enhancement continued to increase, it is likely that the bound water peak was never completely saturated under any of our experimental conditions.

Clot images collected with presaturation at −52 ppm appeared very similar regardless of the nanoparticle treatment (Fig. 5). The clots displayed a uniform hypointensity with respect to the surrounding PBS, most likely as a result of magnetization transfer (MT) from proteins and macromolecules in the clot interacting with bulk water. These interactions widen the water peak resulting in some direct saturation of the bulk water peak even with the presaturation pulse offset by 52 ppm. Despite the MT effect, the surface of clots treated with fibrin-targeted PARACEST nanoparticles could be clearly distinguished after image subtraction. In contradistinction, the surface of clots treated with control nanoparticles could not be discriminated from noise upon subtraction. Averaged over the nine samples, CNR at the clot surface was significantly higher for fibrin-targeted PARACEST nanoparticles (10.0 ± 1.0) compared to the control nanoparticles (2.2 ± 0.4) (* $p < 0.05$).

DISCUSSION

This study presents the incorporation of a bifunctional, asymmetric PARACEST chelate into the surfactant of a fibrin-targeted perfluorocarbon nanoparticle for molecular imaging. Fibrin-targeted PARACEST nanoparticles provide a contrast mechanism that may be activated or deactivated by changing the offset frequency of the presaturation pulse, which allows easy detection of the targeted agent without collecting images before and after contrast administration. In contradistinction to liposomal-based agents which create contrast through a chemical shift effect (11), the contrast mechanism of the fibrin-targeted particles is due to PARACEST interactions.

The importance of detecting and treating unstable plaque before further progression to myocardial infarction or stroke occurs cannot be overstated. Despite the clinical need for this information, the cost, risk, and time required to perform invasive techniques such as intravascular ultrasound (16), thermography (17), and coherent optical tomography (18) have dampened the general enthusiasm for their use beyond the research community. Noninvasive MRI in conjunction with fibrin-targeted molecular imaging agents (3) is positioned to be a favored modality for the detection and characterization of unstable plaque, however, the current need for pre- and post-contrast imaging offset by 30 to 60 minutes is more complicated than desirable. In the future, one could imagine administering a fibrin-targeted PARACEST agent to a patient at the time of presentation and imaging the patient anytime over the next 30 minutes to two hours without interference from circulating contrast or need to have performed a baseline scan before treatment. The practical implication is an earlier diagnosis and treatment, which would be available at lower cost to more patients per available scanner. These clear clinical advantages fuel the mounting research and development interest in PARACEST for molecular imaging.

MT contrast is commonly used in a variety of clinical MRI applications (19). Similar to PARACEST, MT uses a presaturation pulse to suppress some of the signals in the body. While these techniques utilize similar pulse sequences, PARACEST requires a much larger frequency offset and is asymmetric with regards to the bulk water. These differences allow detection of PARACEST agents despite the underlying MT contrast. The hypointense appearance of the clots in Figure 5 probably reflects MT due to the interactions of water molecules with clot proteins. Presaturation at +52 ppm and −52 ppm, however, have identical MT effects, allowing image subtraction to cancel out the MT contributions. No contrast is observed on the subtraction images in areas with MT but no PARACEST particles, such as the clot interior.

LIMITATIONS

While the techniques used in this paper clearly demonstrate PARACEST enhancement with targeted nanoparticles, optimization of the chemistry, coil and pulse sequence is needed to truly capitalize on the strengths of this agent. The Eu^{3+}-methoxy-benzyl-DOTA chelate displayed a bound water peak both in solution as well as coupled to nanoparticles. We did not, however, measure the exchange rate, thus 4.7 T may not be the optimal field strength. In addition, the cationic nature of the PARACEST particles in this study is not desirable in vivo due to the potential interaction with anionic proteins and membranes, which could introduce significant formulation, pharmacokinetic, pharmacodynamics, and biosafety challenges.

We utilized a very simple surface coil, which provided efficient transmission of the saturation pulses. More uniform saturation and sensitivity, however, may be required for in vivo imaging of deep tissues. Moreover, a long, low-power presaturation pulse was inserted into a standard gradient echo imaging sequence, which effectively saturated the bound water

peak, but did not optimize RF deposition or imaging efficiency. Sequences utilizing multi-echo acquisitions or short saturation pulse trains may shorten imaging times and reduce RF deposition. Given the early stage of PARACEST contrast agent development, further research on the chemistry, in vivo particle clearance and several imaging hardware issues is needed. With optimization of the agent and imaging hardware, comparisons between various agents, including CEST agents as well as conventional paramagnetic or superparamagnetic agents (3), can be performed for specific molecular imaging applications.

CONCLUSIONS

This report describes a targeted PARACEST nanoparticle agent with developmental potential for detection of fibrin in unstable atherosclerotic plaques. This agent is particularly attractive because it can be activated through the pulse sequence parameters of the MRI scanner, effectively turning the contrast agent on and off at will. Targeted PARACEST nanoparticles may allow robust detection of contrast agents at a single time point instead of comparing images collected at pre- and post-injection, which would have significant practical benefits in the clinic.

Acknowledgments

The authors thank Dr. Joseph J. H. Ackerman, Professor and Chair, Department of Chemistry, and Director of the Biomedical MR Laboratory at Washington University, for technical assistance and support. This research was supported in part by the NIH (CO-07121, HL-42950, HL-59865 and EB-01704), Philips Medical Systems and the American Heart Association.

References

1. American Heart Association. 2005.
2. Rudd JH, Davies JR, Weissberg PL. Imaging of atherosclerosis -- can we predict plaque rupture? Trends Cardiovasc Med 2005;15(1):17–24. [PubMed: 15795159]
3. Wickline SA, Neubauer AM, Winter P, Caruthers S, Lanza G. Applications of nanotechnology to atherosclerosis, thrombosis, and vascular biology. Arterioscler Thromb Vasc Biol 2006;26(3):435–441. [PubMed: 16373609]
4. Lanza GM, Wallace KD, Scott MJ, Cacheris WP, Abendschein DR, Christy DH, Sharkey AM, Miller JG, Gaffney PJ, Wickline SA. A novel site-targeted ultrasonic contrast agent with broad biomedical application. Circulation 1996;94(12):3334–3340. [PubMed: 8989148]
5. Winter PM, Caruthers SD, Yu X, Song SK, Chen J, Miller B, Bulte JW, Robertson JD, Gaffney PJ, Wickline SA, Lanza GM. Improved molecular imaging contrast agent for detection of human thrombus. Magn Reson Med 2003;50(2):411–416. [PubMed: 12876719]
6. Ward KM, Aletras AH, Balaban RS. A new class of contrast agents for MRI based on proton chemical exchange dependent saturation transfer (CEST). J Magn Reson 2000;143(1):79–87. [PubMed: 10698648]
7. Zhou J, Wilson DA, Sun PZ, Klaus JA, Van Zijl PC. Quantitative description of proton exchange processes between water and endogenous and exogenous agents for WEX, CEST, and APT experiments. Magn Reson Med 2004;51(5):945–952. [PubMed: 15122676]
8. Terreno E, Castelli DD, Cravotto G, Milone L, Aime S. Ln(III)-DOTAMGly complexes: a versatile series to assess the determinants of the efficacy of paramagnetic chemical exchange saturation transfer agents for magnetic resonance imaging applications. Invest Radiol 2004;39(4):235–243. [PubMed: 15021328]
9. Aime S, Delli Castelli D, Terreno E. Supramolecular adducts between poly-L-arginine and [TmIIIdotp]: a route to sensitivity-enhanced magnetic resonance imaging-chemical exchange saturation transfer agents. Angew Chem Int Ed Engl 2003;42(37):4527–4529. [PubMed: 14520757]
10. McMahon MT, Gilad AA, Zhou J, Sun PZ, Bulte JW, van Zijl PC. Quantifying exchange rates in chemical exchange saturation transfer agents using the saturation time and saturation power dependencies of the magnetization transfer effect on the magnetic resonance imaging signal

(QUEST and QUESP): Ph calibration for poly-L-lysine and a starburst dendrimer. Magn Reson Med 2006;55(4):836–847. [PubMed: 16506187]

11. Aime S, Delli Castelli D, Terreno E. Highly sensitive MRI chemical exchange saturation transfer agents using liposomes. Angew Chem Int Ed Engl 2005;44(34):5513–5515. [PubMed: 16052647]
12. Zhang S, Winter P, Wu K, Sherry AD. A novel europium(III)-based MRI contrast agent. J Am Chem Soc 2001;123(7):1517–1518. [PubMed: 11456734]
13. Edgell T, McEvoy F, Webbon P, Gaffney PJ. Monoclonal antibodies to human fibrin: interaction with other animal fibrins. Thromb Haemost 1996;75(4):595–599. [PubMed: 8743185]
14. Raut S, Gaffney PJ. Evaluation of the fibrin binding profile of two anti-fibrin monoclonal antibodies. Thromb Haemost 1996;76(1):56–64. [PubMed: 8819252]
15. Tymkewycz PM, Creighton Kempsford LJ, Gaffney PJ. Generation and partial characterization of five monoclonal antibodies with high affinities for fibrin. Blood Coagul Fibrinolysis 1993;4(2): 211–221. [PubMed: 7684615]
16. Escolar E, Weigold G, Fuisz A, Weissman NJ. New imaging techniques for diagnosing coronary artery disease. Cmaj 2006;174(4):487–495. [PubMed: 16477061]
17. Toutouzas K, Drakopoulou M, Stefanadi E, Siasos G, Stefanadis C. Intracoronary thermography: does it help us in clinical decision making? J Interv Cardiol 2005;18(6):485–489. [PubMed: 16336430]
18. Regar E, Schaar JA, Mont E, Virmani R, Serruys PW. Optical coherence tomography. Cardiovasc Radiat Med 2003;4(4):198–204. [PubMed: 15321058]
19. Rumboldt Z, Marotti M. Magnetization transfer, HASTE, and FLAIR imaging. Magn Reson Imaging Clin N Am 2003;11(3):471–492. [PubMed: 14768730]

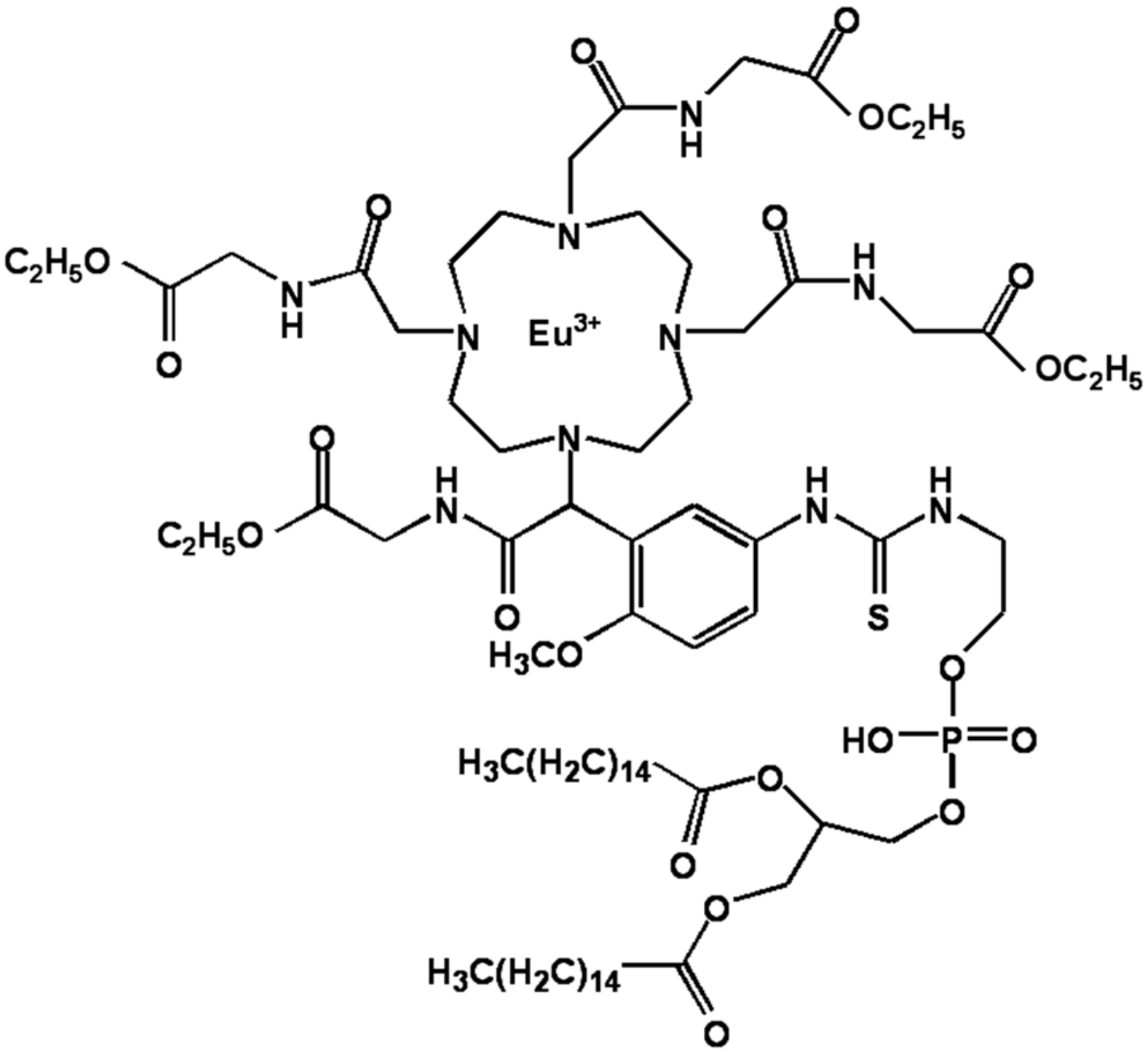

FIG. 1.

Chemical structure of lipid conjugated PARACEST contrast agent. Eu^{3+} is chelated to methoxy-benzyl-DOTA, which is functionalized with a phospholipid moiety for incorporation into the lipid membrane of perfluorocarbon nanoparticles.

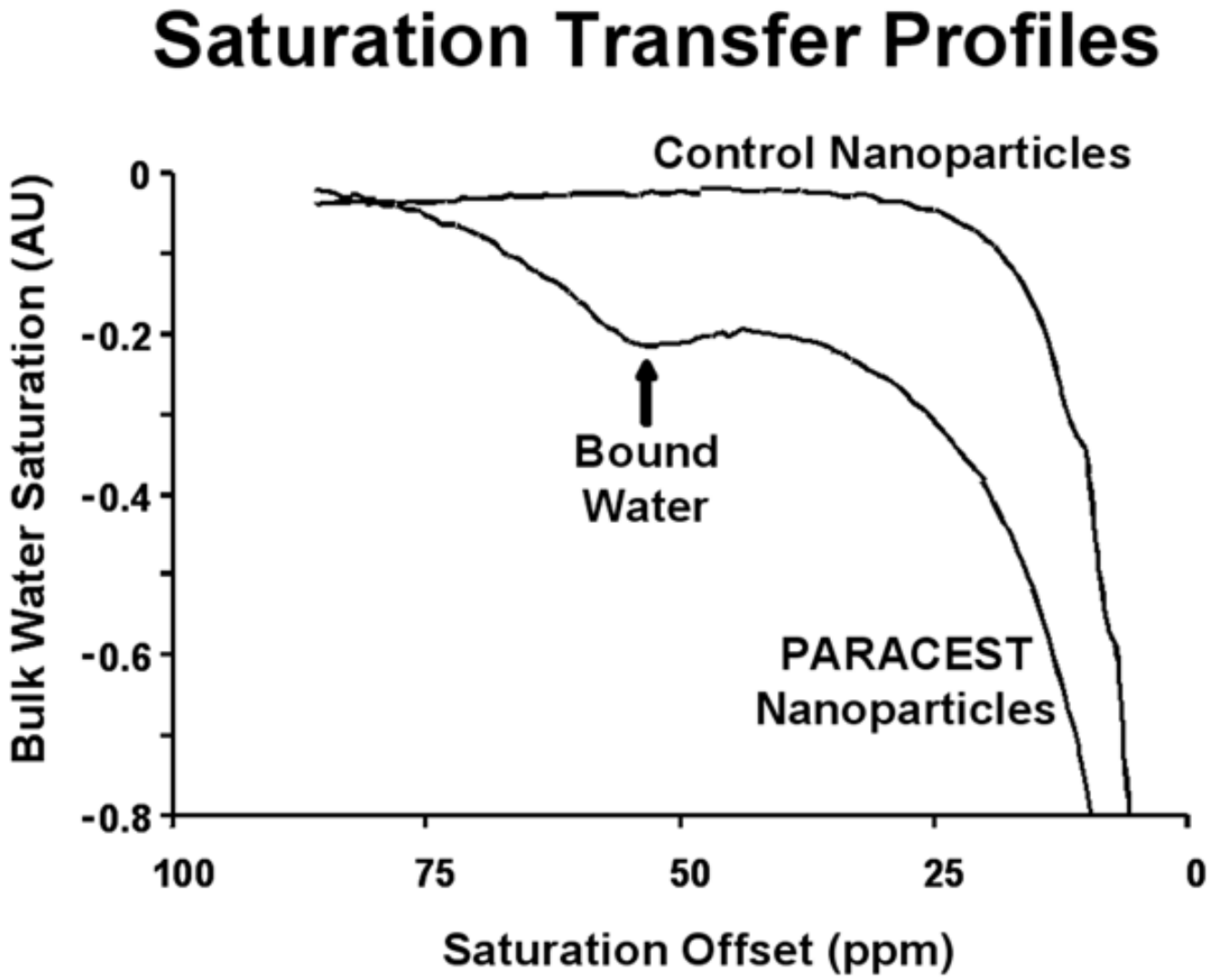

FIG. 2.

Saturation profile of PARACEST nanoparticles shows a clear saturation transfer effect at 52 ppm (arrow) confirming saturation of the bound water peak and effective transfer of magnetization. Control nanoparticles do not show any saturation transfer effects at this chemical shift.

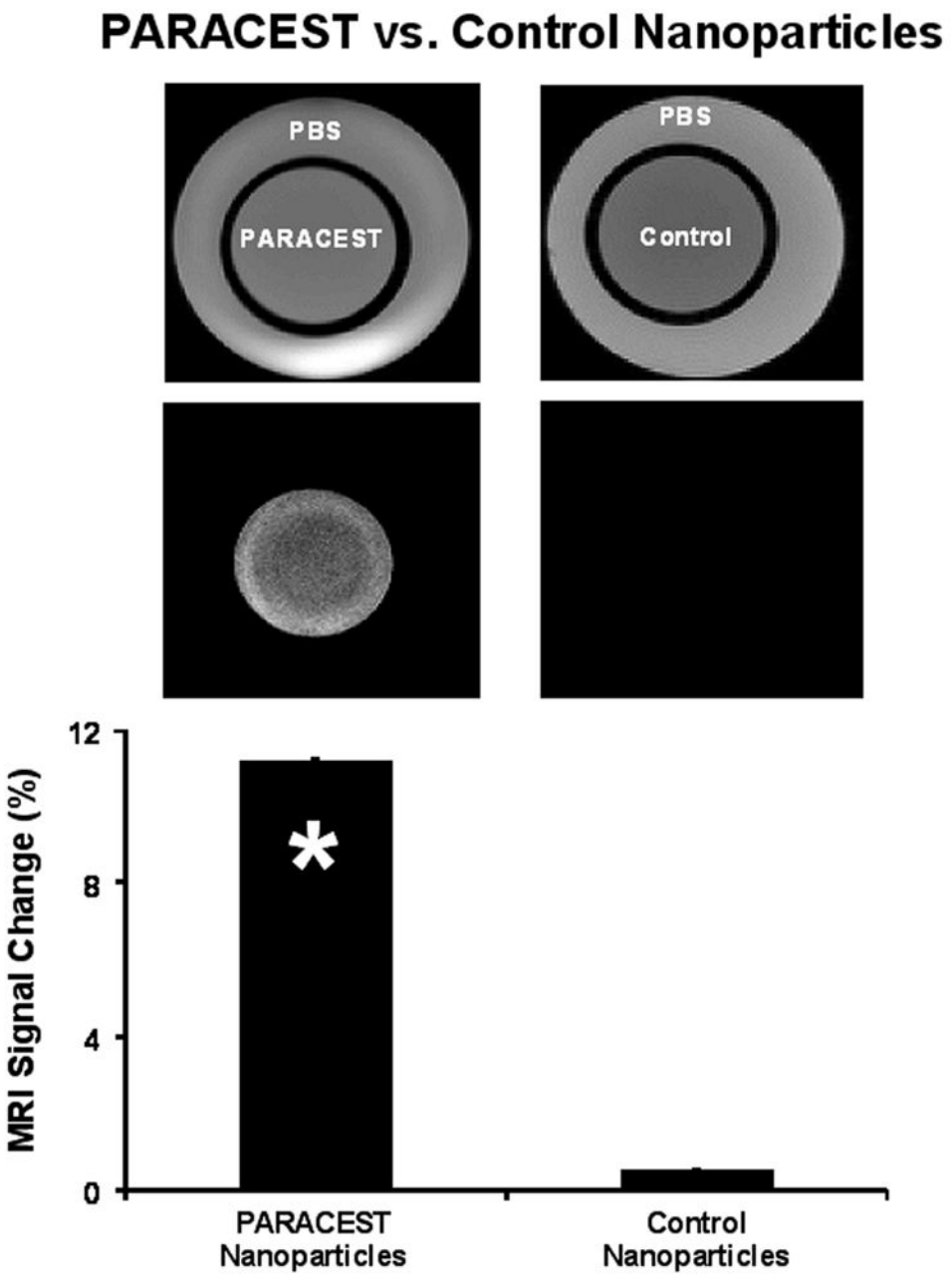

FIG. 3.

Imaging of two-chambered phantom containing PARACEST nanoparticles (left) or control nanoparticles (right) in the inner chamber and PBS in the outer chamber. Original images collected with saturation at −52 ppm (top) show no differences between PARACEST and control nanoparticles. Subtraction images (middle) reveal uniform signal enhancement in the PARACEST chamber and no enhancement in the outer PBS chambers or with control nanoparticles. The signal enhancement (bottom) in the PARACEST nanoparticle chamber was significantly higher than control nanoparticles (* $p < 0.05$).

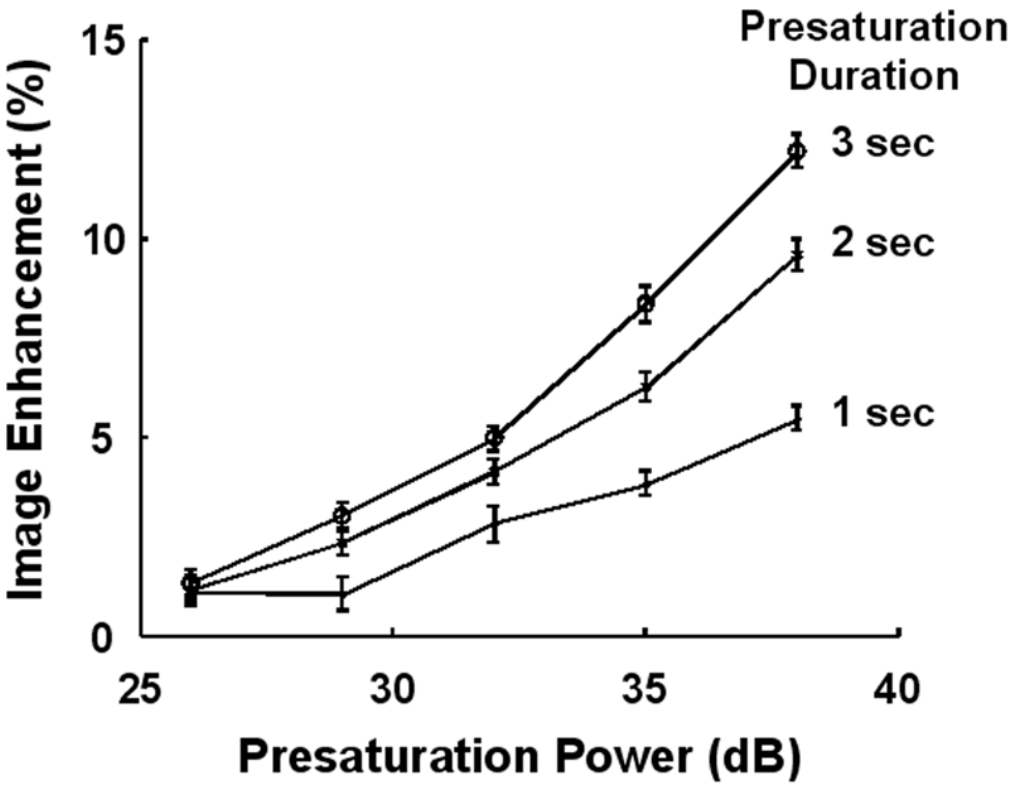

FIG. 4.

Increasing the power or duration of the saturation pulse increases the signal enhancement obtained from PARACEST nanoparticles. Presaturation pulses as short as 1 second can produce a 5% change in image intensity.

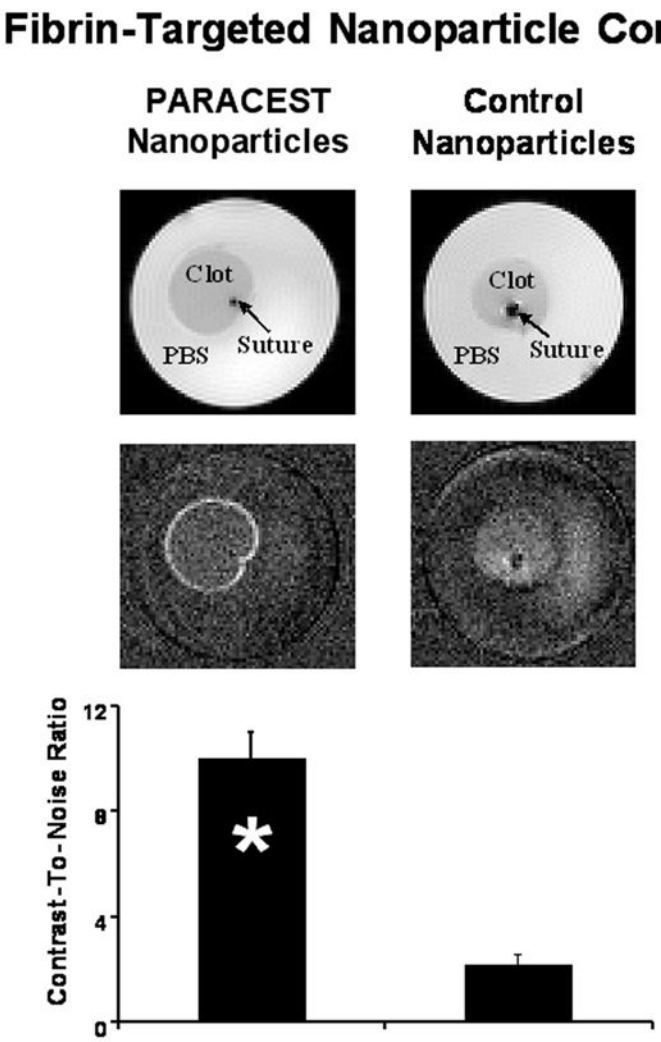

FIG. 5.

Imaging of fibrin-targeted PARACEST (left) or control (right) nanoparticles bound to plasma clots. Images obtained with saturation at −52 ppm (top) show no differences between clots treated with PARACEST or control nanoparticles. Subtraction images (middle) reveal signal enhancement on the surface of the clot treated with PARACEST nanoparticles and no enhancement of the clot treated with control nanoparticles. The CNR calculated at the clot surface (bottom) was significantly higher with PARACEST nanoparticles compared to control nanoparticles (* $p < 0.05$).